Promotion of glacial ice sheet buildup 60–115 kyr B.P. by precessionally paced Northern Hemispheric meltwater pulses

A. Timmermann,[1] J. Knies,[2] O. Elison Timm,[1] A. Abe-Ouchi,[3] and T. Friedrich[1]

Received 20 January 2010; revised 21 May 2010; accepted 15 June 2010; published 28 October 2010.

[1] Compared to the rapid glacial terminations, the buildup of glacial ice sheets in the Northern Hemisphere took tens of thousands of years. During the buildup phase, the growing ice sheets were subject to major orbitally induced summer insolation changes, without experiencing complete disintegration. The reason for this behavior still remains elusive. Here we propose that between 110 and 60 kyr B.P., every ~20 kyr increased summer insolation in high northern latitudes triggered massive instabilities of the Northern Hemispheric ice sheets, leading to glacial meltwater pulses and subsequent disruptions of the Atlantic Meridional Overturning Circulation (AMOC). Associated severe cooling of the northern extratropics may have offset the warming trends driven by increased precessional summer insolation. This temperature response diminished the melting trend and stabilized the ice sheets. Our results suggest that the competition between the direct insolation changes and the indirect climate responseto AMOC disturbances may be an important negative feedback that supports the buildup of glacial ice sheets.

Citation: Timmermann, A., J. Knies, O. E. Timm, A. Abe-Ouchi, and T. Friedrich (2010), Promotion of glacial ice sheet buildup 60–115 kyr B.P. by precessionally paced Northern Hemispheric meltwater pulses, *Paleoceanography*, *25*, PA4208, doi:10.1029/2010PA001933.

1. Introduction

[2] Late Pleistocene climate variations were dominated by glacial-interglacial cycles, with typical time scales of 80–120 kyr [*Hays et al.*, 1976]. The climate system has spent only a short time in interglacial periods, such as the penultimate interglacial (Eemian) or the recent Holocene, whereas glacial conditions prevailed for more than 80% of the time. While positive feedbacks accelerated orbitally induced summer melting of glacial ice during glacial terminations the relatively slow buildup of glacial ice sheets and the subsequent subsidence of the ice sheet into the lithosphere are slow processes, characterized by time scales in the order of tens of thousand of years [*Oerlemans*, 1980; *Gallée et al.*, 1992]. The physical mechanisms responsible for this apparent asymmetry and the resulting sawtooth-like structure of ice volume changes have not been fully understood yet.

[3] Recent geological evidence [*Svendsen et al.*, 2004; *Larsen et al.*, 2006] supports the notion that during the early stages of the last glacial period the northern Eurasian ice sheet reached its maximum extent earlier than the Laurentide ice sheet. The former attained its maximum size already around 90 kyr B.P., while the latter continued to grow [*Dyke et al.*, 2002] for another 70 kyr. During the initial buildup of the Eurasian ice sheet around 115 kyr B.P. relatively warm climate conditions prevailed in the Nordic Seas. Such conditions were probably associated with an intensified AMOC [*Risebrobakken et al.*, 2007] and increased atmospheric moisture convergence [*Siegert et al.*, 2001]. Large proglacial lakes along the southern rim of the Eurasian ice sheet have been suggested as additional boosters for the fast glacial buildup [*Krinner et al.*, 2004; *Peyaud et al.*, 2007] by providing enough thermal inertia to reduce summer surface air temperatures.

[4] Data and modeling results [*Peyaud et al.*, 2007] further document that the base of the Barents–Kara Sea ice sheet portion of the Eurasian ice sheet was below sea level. Marine-based ice sheets are highly vulnerable to external forcing [*Oppenheimer*, 1998], such as, e.g., orbitally induced ocean warming and sea level changes. Terrestrial and marine archives [*Mangerud et al.*, 2004; *Svendsen et al.*, 2004; *Spielhagen et al.*, 2004] from northern Eurasia provide evidence for early glacial ice sheet instabilities. Well-constrained events around 65 kyr, 87 kyr, 108 kyr B.P. (also known as Heinrich 6, C21, C24) were accompanied by Arctic ice-rafted detritus (IRD) layers (Figure 1d), planktic δ^{13}C anomalies [*Spielhagen et al.*, 2004] (Figure 1e) and planktic δ^{18}O anomalies [*Knies et al.*, 2007] in the Arctic Gateway region (not shown). These data are consistent with the occurrence of early glacial freshwater pulses, originating from the northern Eurasian ice sheet and discharging into the Arctic–North Atlantic gateway region [*Knies et al.*, 2007]. They occurred simultaneously with positive trends in boreal summer insolation (Figure 1a), and IRD layers further south in the North Atlantic [*Chapman and Shackleton*, 1999; *Oppo et al.*, 2006] (Figures 1b and 1c). The transport

[1]IPRC, SOEST, University of Hawaii, Honolulu, Hawaii, USA.
[2]Geological Survey of Norway, Trondheim, Norway.
[3]Atmosphere and Ocean Research Institute, University of Tokyo, Kashiwa, Japan.

0883-8305/10/2010PA001933

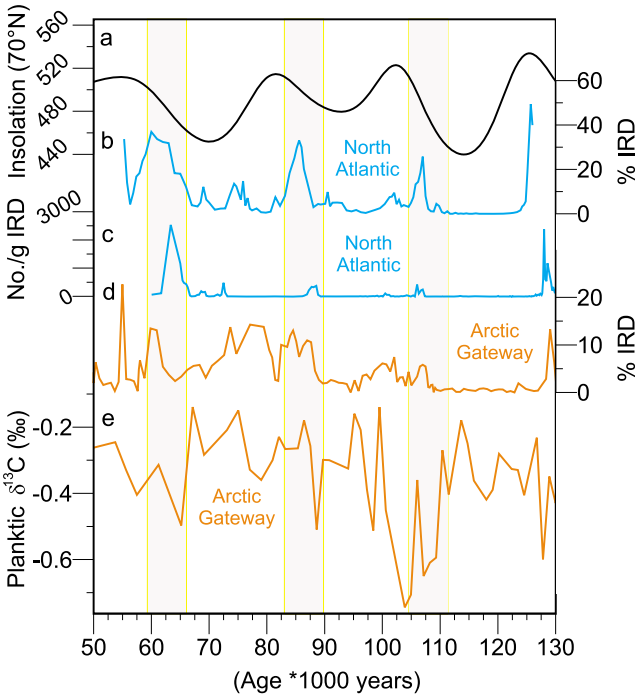

Figure 1. Climate proxy data from the North Atlantic and Arctic gateway region. (a) Summer insolation (15 June) [*Berger*, 1978] at 70°N. (b) North Atlantic IRD data [*Chapman and Shackleton*, 1999] from sediment core NEAP18K (fraction > 150 μm) at 52.8°N and 30.35°W. (c) IRD data from EW9302-JPC8 data [*Oppo et al.*, 2001] at 61°N, 25°W. (d) Arctic gateway IRD data [*Knies and Vogt*, 2003] (fraction > 250 μm) from the northern Barents Sea margin (gravity core PS2138, position 81°32.1′N; 30°25.6′E; 995 m water depth). (e) δ^{13}C isotope data of planktic foraminifera N. pachyderma sin. from the Yermak Plateau [*Knies et al.*, 2007] (ODP Hole 910A, position 80°15.882′N, 6°35.405′E, 556.4 m water depth). Periods of gradually increasing summer insolation that coincided with major meltwater pulses are highlighted in grey. The chronology is compiled from individual age models given in the respective references.

of the Arctic meltwater signal via the Transpolar Drift into the Nordic Seas caused freshening and eventually a reduction of deep-water formation, as evidenced by concurrent decreases of benthic δ^{13}C values (Figure 2b), and cooling of the North Atlantic region (Figure 2d).

[5] Whether the reported meltwater pulses during MIS5 were potent enough to induce a near-complete glacial termination of the Eurasian and Laurentide ice sheets as suggested by recent speleothem-based sea level reconstructions [*Dorale et al.*, 2008] for MIS5a is still controversial. In fact, current sea level reconstructions for MIS5 disagree by up to 40 m [*Siddall et al.*, 2003; *Thompson and Goldstein*, 2005; *Dorale et al.*, 2008] which hampers any effort to properly constrain the full extent and evolution of the Eurasian and Laurentide ice sheets.

[6] Based on the observational findings documented in Figures 1 and 2 and acknowledging the uncertainty in current MIS5 sea level estimates we formulate the following hypothesis for the early glacial ice sheet buildup: every ~20 kyr orbitally induced instabilities of the northern ice sheets and the subsequent weakening of the thermohaline circulation helped to offset the effects of increased summer insolation (Figure 1a), thereby creating conditions favorable for further growth of Northern Hemispheric ice sheets and providing an important negative feedback.

[7] Updated and more refined future sea level reconstructions for MIS5 will have the potential to prove our hypothesis wrong or lend further supporting evidence.

2. Methods

[8] To test this hypothesis several sensitivity experiments are conducted using the earth system model of intermediate

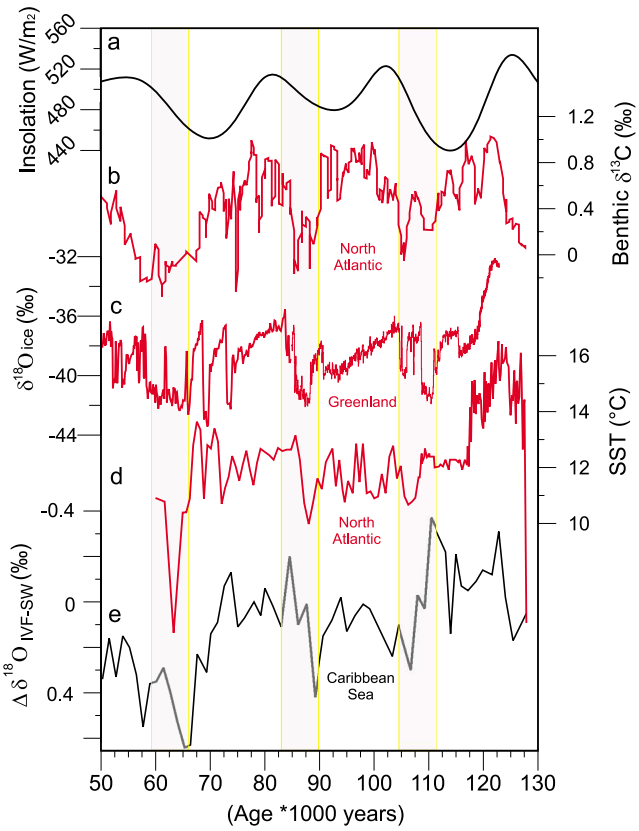

Figure 2. North Atlantic climate response to precessional meltwater pulses during the early glacial period. (a) Summer insolation [*Berger*, 1978] at 70°N. (b) Stable carbon isotope data of benthic foraminifera from the North Atlantic [*Curry and Oppo*, 1997]. (c) Stacked record of Greenland ice core δ^{18}O data (GISP2 [*Stuiver and Grootes*, 2000] 50–84 kyr and NGRIP [*North Greenland Ice Core Project Members*, 2004] 84–123 kyr). (d) North Atlantic sea surface temperature data [*Oppo et al.*, 2006]. (e) Paleosalinity data ($\Delta\delta^{18}$O ice volume − sea water) from the Caribbean Sea [*Schmidt et al.*, 2004]. The chronology is derived from individual age models given in each reference as in Figure 1.

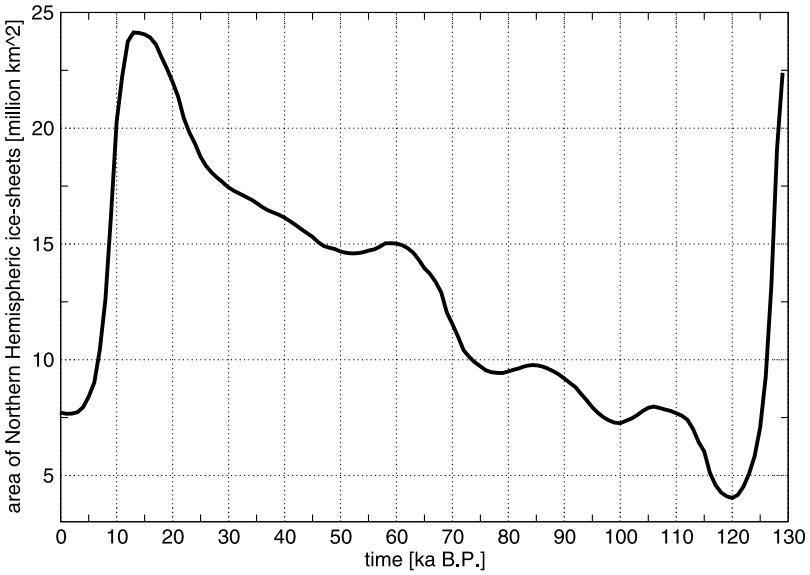

Figure 3. Simulated evolution of ice sheet area (million km^2) 0–130 kyr B.P. using the IcIES ice sheet model [*Abe-Ouchi et al.*, 2007].

complexity LOVECLIM [*Driesschaert et al.*, 2007; *Renssen et al.*, 2005; *Timm and Timmermann*, 2007].

[9] It consists of 5 coupled subsystems: a simplified 3-layer global atmosphere, a 3-D global ocean model and a thermodynamic-dynamic sea ice model, a terrestrial vegetation and a biogeochemical carbon cycle model. For our purposes we deactivated the coupling of the climate components with the vegetation model and the carbon cycle model.

[10] The global atmospheric model is based on a quasi-geostrophic adiabatic core with T21 resolution and three vertical layers. Ageostrophic forcing terms are diagnosed from the vertical motion field. These terms are added to the prognostic vorticity equation and the thermodynamic equation, which improves the Hadley circulation. A linear balance equation that links geopotential height and vorticity and that neglects the effect of divergent winds is used. A set of physical parameterizations of diabatic processes (radiative fluxes, sensible and latent heat fluxes) is included. The diabatic heating is incorporated in the thermodynamic equation. The radiation scheme uses a linearization with respect to present day conditions. The seasonally and spatially varying cloud cover climatology is prescribed in the model.

[11] The ocean model CLIO [*Goosse et al.*, 1999; *Goosse and Fichefet*, 1999] is a three-dimensional primitive equation model on z coordinates with a free surface. It is coupled to a thermodynamic-dynamic sea ice model. The horizontal resolution is 3° × 3°. The globe is covered by a partly rotated grid in the North Atlantic sector. In vertical direction, the model is divided into 20 unevenly spaced levels. Vertical mixing, mixing along isopycnals, the effect of mesoscale eddies on transports and mixing, and downsloping currents at the bottom of continental slopes are parameterized. In our simulations the effect of glacial interglacial sea level changes on the bathymetry and on the seawater salinity is neglected. The Bering Strait is closed in the simulations.

[12] The three physical components of LOVECLIM (atmosphere, ocean, sea ice) are coupled by exchange of momentum, heat, freshwater. The hydrological cycle is closed over land by a bucket model for soil moisture, and river runoff into the ocean.

[13] Ice sheet forcing in the LOVECLIM model is taken into account through changes in the orography and in the surface albedo. For the transient simulation TR, covering the past 130 kyr, the ice sheet orography and albedo anomalies follow a time-dependent off-line ice sheet simulation [*Abe-Ouchi et al.*, 2007] obtained with the IcIES model in 1° × 1° resolution. IcIES uses the shallow ice approximation, couples ice sheet dynamics with lithospheric thermal and dynamical processes and simulates the glacial-interglacial changes in global ice volume and area quite realistically (Figure 3).

[14] In the transient LOVECLIM climate model simulation time-varying atmospheric CO_2 concentrations are prescribed according to the Antarctic Taylor Dome [*Indermühle et al.*, 1999; *Smith et al.*, 1999] ice core data. The daily mean irradiance is calculated following astronomical theory [*Berger*, 1978]. The 130 kyr transient simulation uses accelerated orbital forcing. With an acceleration factor of 20 the transient glacial-interglacial simulation reduces to 6,500 model years. One of the main advantages of this technique is to save computing time. Disadvantages related to the mismatch between accelerated forcing and slow equilibration processes in the climate system have been previously studied [*Timm and Timmermann*, 2007; *Timm et al.*, 2008].

[15] Using the boundary conditions of 108 kyr B.P. and the initial state of the transient accelerated simulation [*Timm et al.*, 2008], an unaccelerated waterhosing experiment WH is conducted to study the effect of Northern Hemispheric

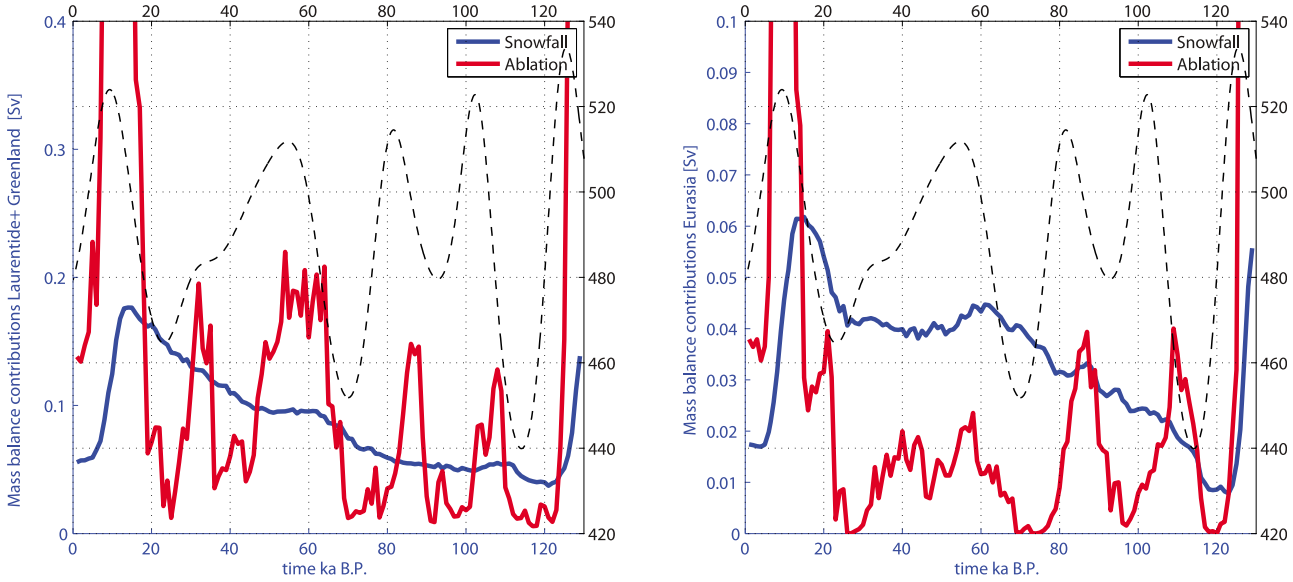

Figure 4. (left) Simulated freshwater balance over Laurentide and Greenland ice sheet in the transient climate model experiment TR: spatially integrated snowfall changes (blue) and ablation anomalies (red) (computed from the positive degree days simulated in TR). Boreal summer insolation at 70°N is represented by a black dashed line. (right) Same as Figure 4 (left), but for the Eurasian ice sheet.

meltwater pulses on the climate during Marine Isotope Stage 5. Freshwater forcing in the northern North Atlantic (between 50°N and 70°N) is linearly increased for 500 years attaining a maximum value of 0.35 Sv and then decreased for another 500 years.

3. Results

[16] The mass balance of the glacial ice sheets and hence their temporal evolution are very sensitive to temperature over the ablation zone, insolation and precipitation over the whole ice sheet area.

[17] To estimate the effect of orbitally induced insolation changes on the ice sheets during MIS4 (60–75 kyr B.P.) and MIS5a–d (75–115 kyr B.P.), we calculated the mass balance of the ice sheets from the transient modeling experiment TR a posteriori. This was done in the following way. First, annual mean snowfall was diagnosed over the 130 kyr forcing period over the ice sheet regions. Then, using absolute surface temperature values we calculated the Positive Degree Days (PDDs) for every year and the corresponding ablation (note, however, that the TR simulation does not experience this a posteriori diagnosed meltwater forcing, nor does the IcIES simulation) using the parameterization of *Reeh* [1991]. To account for temperature biases in LOVECLIM with respect to the observational record we introduced an offset of 2°C that the simulated LOVECLIM 2m temperature must exceed to be included in the yearly accumulation of PDDs.

[18] The individual contributions to the diagnosed mass balance over the ice sheet are shown for the Laurentide (Figure 4, left) and Eurasian (Figure 4, right) ice sheets. For termination II (130–125 kyr B.P.) massive ablation anomalies attain very large values of more than 1 Sv and exceed the annual snow accumulation for the Laurentide ice sheet. The resulting very large negative mass balance could be interpreted as the meltwater pulse associated with Heinrich event 11 (H11) and as the trigger for termination II. There are two reasons for the high diagnosed values of ablation between 130 and 125 kyr B.P. in experiment TR: increased external radiative forcing (orbital and greenhouse gasses) as well as decreasing ice sheet height and hence surface warming in the IcIES model simulation that is used as a boundary forcing for experiment TR generate large values of PDD. Very low summer insolation values around 118–112 kyr B.P. reduce the number of PDDs for both the Laurentide and Eurasian ice sheets.This feature triggers the glacial inception. Although snowfall anomalies are relatively small, they still exceed the diagnosed ablation rate during this time. Increasing summer insolation around 110–102 kyr B.P. leads to a rapid increase of PDDs and large diagnosed ablation values for both Northern Hemispheric ice sheets. The resulting net mass balance (snowfall minus ablation) for the Laurentide+Greenland and Eurasian ice sheets attains values of 0.07 and 0.02 Sv for several thousand years, respectively (Figure 5).

[19] A similar situation to 110–102 kyr B.P. is found during MIS5b (93–82 kyr B.P.): boreal summer insolation increases, resulting in positive ablation anomalies that exceed the simulated snowfall for the Laurentide ice sheet. The net result is a meltwater pulse, as documented in Figure 5 which coincides with the observed meltwater pulse C21. Corresponding global sea level changes amount to about 20 m. The Eurasian ice sheet releases only a small meltwater pulse that does not contribute much to the overall sea level rise during this period. Another precessionally forced increase of meltwater discharge is observed around 65 kyr B.P. and corresponds to Heinrich event 6.

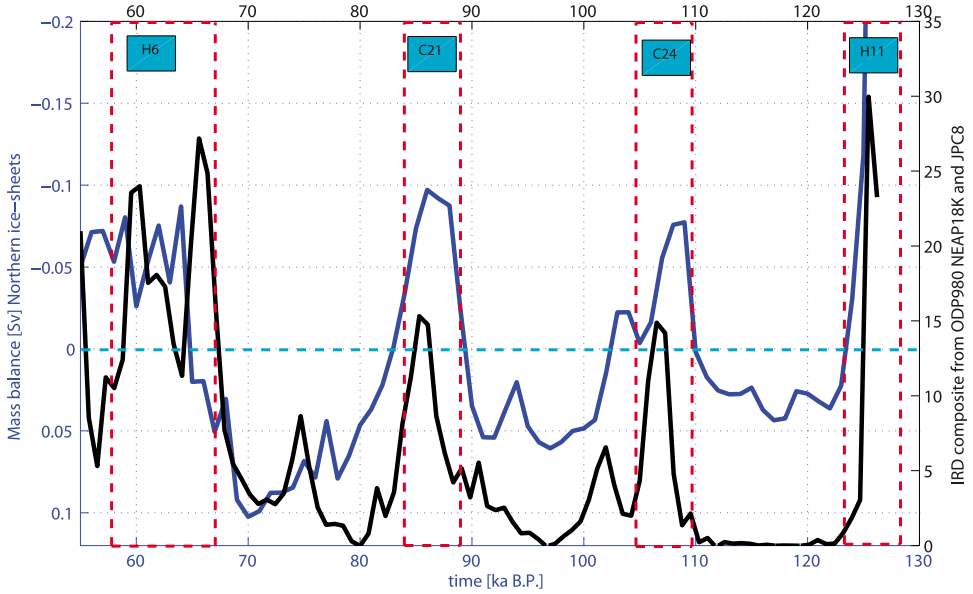

Figure 5. Mass balance values (Sv) for Northern Hemispheric ice sheets obtained from experiment TR using simulated annual snowfall, ablation (computed from the simulated positive degree days), and the ice sheet areas obtained from an off-line IcIES simulation that was used as a topography and albedo forcing for TR. (black) Composite of North Atlantic IRD data from sediment cores NEAP18K, ODP908, and JPC8 (all interpolated onto an equidistant time axis using their individual age scales).

[20] MIS3 is characterized by a lack of strong precessional variability in Northern Hemispheric summer insolation. This may leave enough freedom for the ice sheets to develop their own instabilities with time scales of 8–10 kyr. Witnesses to these instabilities are Heinrich events 2–4. The LOVECLIM simulation TR, on the other hand, simulates a precessionally paced meltwater pulse at 35 kyr B.P. In fact this meltwater discharge event roughly coincides with the observed Heinrich event 4. Heinrich events 2 and 3 do not correlate with the summer insolation changes.

[21] The next large swing in summer insolation occurs around 20 kyr B.P. Together with the overall concurrent increase of CO_2 concentrations, this leads to a massive simulated increase in ice sheet ablation at a time that coincides roughly with Heinrich event I (Figure 4). The resulting simulated negative mass balance values are sufficient to trigger a glacial termination. Calving and other fast ice sheet processes would certainly contribute to these large anomalies.

[22] The mass balance calculated from the LOVECLIM simulation TR is certainly not a very accurate representation of what really happened during the last glacial period, but it gives some qualitative insight into the competing effects of snowfall and temperature and how they may have shaped the evolution of the glacial ice sheets during the last 130 kyr.

[23] One noteworthy feature of our simulations is the fact that during MIS4,5 they provide a skilful "hindcast" of the reconstructed meltwater events H6, C21, C24, H11 which were accompanied by large IRD anomalies (Figure 5). IRD events are typically associated with ice sheet and/or ice shelf instabilities that release icebergs into the North Atlantic. This can in principle happen independently from large-scale ice sheet melting induced by summer insolation changes. However, the coincidence found here between reconstructed North Atlantic IRD anomalies and simulated meltwater pulses may suggest that there is a physical connection. Several scenarios are plausible and should be studied in more detail:

[24] 1. Summer ice sheet melting and the associated sea level rise destabilize the ice shelves, thereby releasing icebergs from the shelves and adjacent coastal glaciers.

[25] 2. Summer melting at lower elevations generates meltwater ponds that could quickly drain through moulins to the base of the ice sheet base. Lubrication near the base accelerates ice flow toward the ocean, which may eventually trigger a surge of icebergs.

[26] 3. Precessionally paced ocean warming may lead to a retreat of the ice sheet grounding line, which will result in an increase of iceberg discharge.

[27] 4. Summer insolation anomalies change the mass balance of the ice sheet and independently shift the polar front, which will affect the survivability of icebergs in the North Atlantic.

[28] As already suggested by Figures 1 and 2, meltwater pulses H6 (~62 kyr B.P.), C21 (~86 kyr B.P.), C23 (~102 kyr B.P.), C24 (108 kyr B.P), and C25 (109 kyr B.P.) were accompanied by major changes of North Atlantic ocean ventilation. In fact the corresponding benthic $\delta^{13}C$ anomalies for these events are comparable to Heinrich event I. An important question that needs to be addressed is what processes prevented a runaway termination during phases of increased summer insolation during MIS4, MIS5a–d that

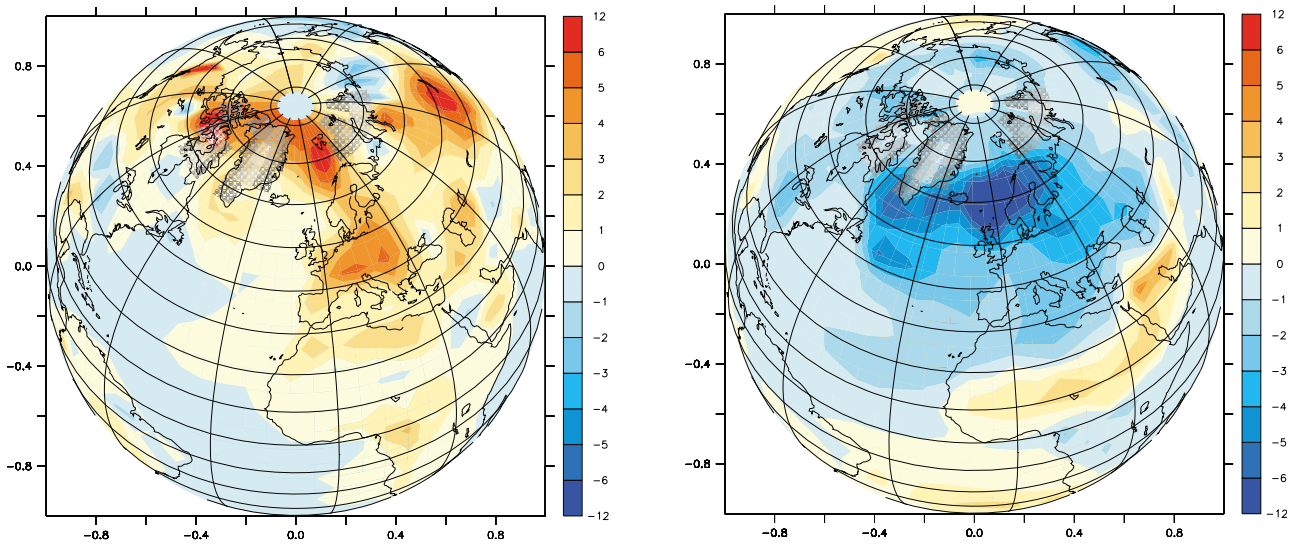

Figure 6. (left) Boreal summer surface temperature difference (K) between 102 kyr B.P. and 114 kyr B.P. simulated by the accelerated transient climate model experiment TR that uses time-varying ice sheet albedo and orography, greenhouse gas concentrations, and orbital forcing [*Timm and Timmermann*, 2007]. (right) Boreal summer mean (June–August) surface temperature difference (K) between a collapsed AMOC state at 108 kyr B.P. and a 108 kyr B.P. background control simulation. The difference is based on 100 year means centered around the state of the maximum of the freshwater forcing in WH and a 100 year mean of the 108 kyr B.P. control run.

were comparable in magnitude to the insolation change that accompanied the last glacial termination. According to Figure 5 the diagnosed negative net mass balance values for the Northern Hemispheric ice sheets during ~85 kyr B.P. and ~108 kyr B.P. attained values of about 0.1 Sv which is comparable in magnitude to *Ganopolski et al.* [2009]. With a duration of about 5 kyr these pulses could each have released an equivalent of 20–30 m global sea level rise which may have been enough to severely reduce the size of the early MIS5 ice sheets which stored a total water volume equivalent to ~20–40 m [*Siddall et al.*, 2003; *Thompson and Goldstein*, 2005].

[29] Numerous observational and modeling studies have demonstrated [e.g., *Stouffer et al.*, 2006] that a weakening of the AMOC, such as during H6, C21, C24, leads to a substantial cooling of the Northern Hemisphere. Here we try to quantify whether this widespread year-round cooling may have helped to partly offset the summer warming and reduce the precessionally driven ablation anomalies.

[30] Experiment WH uses the climate background conditions (greenhouse gasses, orbital forcing, albedo and orography forcing from IcIES) that correspond to 108 kyr B.P. and mimics meltwater pulse C24 by artificially increasing the freshwater flux into the northern North Atlantic for these boundary conditions. Our freshwater forcing is highly idealized and was chosen to trigger a shutdown of the AMOC, in accordance with the benthic δ^{13}C data shown in Figure 1. As expected, the collapse of the AMOC leads to an extensive Northern Hemispheric cooling (Figure 6, right), in accordance with paleoproxy evidence (Figure 2).

[31] The simulated boreal summer cooling (Figure 6, right) is most prominent over the North Atlantic and Eurasia. Compared to the unperturbed background conditions at 108 kyr B.P., the resulting change in diagnosed ablation over the Laurentide and Eurasianice sheets amount to about 75%. The increase in summer temperatures over Eurasia from 102 kyr B.P. to 114 kyr B.P. (Figure 6, left) can be compensated for by the temperature response to the AMOC shutdown (Figure 6, right). The zero degree isotherm shifts by several degrees in latitude during WH (not shown). To further illustrate the effect of AMOC changes on the ice sheet mass balance during MIS5 we assume that the benthic δ^{13}C time series in Figure 2 is a manifestation of changes in the strength of the AMOC. This notion is indirectly supported by the bipolar seesaw behavior of North Atlantic and Antarctic temperatures during MIS5 [*Capron et al.*, 2010]. Accordingly, the benthic δ^{13}C time series in Figure 1 is scaled such that the negative value at 83 kyr B.P. corresponds to 0.25 (representing the PDD decrease of 75% during an AMOC shutdown) and the values of δ^{13}C = 0.8 corresponds to 1. The resulting time series is multiplied as a scaling factor to the diagnosed ablation for the Laurentide and Eurasian ice sheets in the TR experiment (note that we have neglected the effect of the relatively small snowfall changes over the icesheets during the AMOC weakening on the mass balance). The results are shown in Figure 7. As a result of the AMOC cooling effect we observe a major decrease of diagnosed meltwater discharge during H6, C21, C24. Instead of sea level changes of 20–30 m, the AMOC effect reduces the net meltwater discharge of the Laurentide ice sheet by about 50%. For the Eurasian ice sheet the net mass balance during MIS4, MIS5a–d is almost always positive, if AMOC changes are accounted for. Hence the AMOC

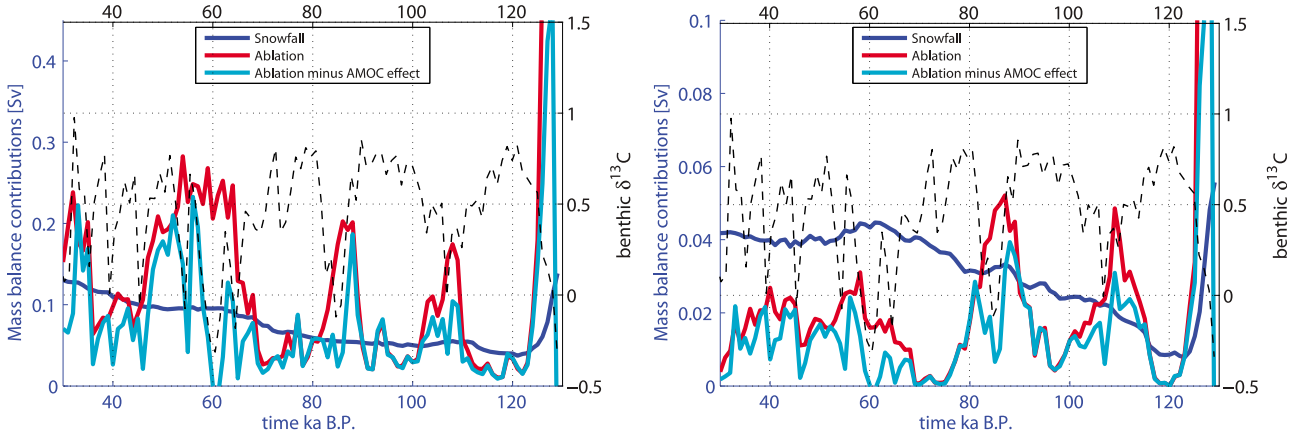

Figure 7. MIS4 and MIS5. (left) Simulated freshwater balance over Laurentide and Greenland ice sheet in the transient climate model experiment TR. Spatially integrated snowfall changes (blue) and ablation anomalies (red) (computed from the positive degree days simulated in TR) and ablation anomalies that include the effect of the AMOC weakening (cyan) (obtained by subtracting the empirically scaled benthic δ^{13}C record from the simulated ablation time series; the scaling factor was chosen so as to obtain a reduction of ablation values by 0.75 for AMOC shutdown, in accordance with experiment WH). (black dashed) δ^{13}C from North Atlantic [*Curry and Oppo*, 1997]. (right) Same as Figure 7 (left), but for the Eurasian ice sheet.

cooling effect is enough to significantly stabilize both ice sheets and reduce the risk of early glacial terminations.

4. Summary and Discussion

[32] Orbitally induced high latitude summer insolation changes during MIS5a–d attained similar absolute values as during the glacial termination phase between 21 kyr B.P. and 10 kyr B.P. Yet, a complete disintegration of the Northern Hemispheric ice sheets did not occur during this initial buildup phase of the glacial ice sheets.

[33] Analyzing paleoproxy data and climate model simulations, we identified the following mechanisms that may have helped to promote the buildup of the glacial ice sheets: Phases of increased boreal summer insolation during Marine Isotope Stage 4–5a to 5e (~59–130 kyr B.P.) caused melting of the northern ice sheets on a precessional time scale and a subsequent weakening of the AMOC. The North Atlantic cooled in response to the reduced poleward oceanic heat transport, thereby offsetting the orbitally induced summer warming in high latitudes. This may have stabilized in particular the Eurasian ice sheet against precessionally induced ablation anomalies.

[34] The negative climate feedback identified here may play an important role in the buildup phase of the glacial ice sheets during MIS4,5a–d (55–120 kyr B.P.). The AMOC cooling effect reduces the ablation on both ice sheets substantially (by up to 75%). A simple empirical model that was scaled to the LOVECLIM mass balance during an AMOC shutdown (experiment WH) demonstrated that the accumulated meltwater discharge for the Heinrich 6, C21 and C24 events is reduced by 50% (see Figure 7). Without the AMOC effect the diagnosed accumulated Northern Hemispheric net mass balance for each of the events C21 and C24 amounts to about 20 m global sea level equivalent. According to sea level reconstructions [*Siddall et al.*, 2003], global sea level during MIS5a–d was about 40 m below the present level. A negative accumulated mass balance anomaly of 20 m during C21, in particular, could have easily shifted the Laurentide and Eurasian ice sheets to the verge of disappearance. Including the AMOC effect on ablation reduces this number by about 50%. This is likely to have a substantial effect on the buildup of the ice sheets during MIS5a–d.

[35] How the identified negative feedback translates to glacial terminations, such as Termination I is unclear. Clearly the AMOC response to freshwater forcing is nonlinear. Hence the proposed negative feedback may saturate for strong freshwater forcing. Therefore, for situations such as Heinrich event I, the climate response to other forcings such as increases in boreal summer insolation and greenhouse gas concentrations may easily outweigh the saturated negative AMOC ice sheet feedback and lead to a complete termination, in contrast to MIS5.

[36] Our model results also demonstrated the crucial importance of precessional forcing for the buildup and termination of glacial ice sheets. Major meltwater events, including H11 and H1, can be directly hindcasted from the diagnosed mass balance in the LOVECLIM 130 kyr simulation. In TR ablation anomalies occur in response to precessional forcing in boreal summer, greenhouse gas changes, the retreat of the ice sheets via the ice albedo effect and the lapse rate effect.

[37] Other mechanisms have been described that may prevent the collapse of the relatively small glacial ice sheets during MIS5a–5d, such as the “Small Ice Cap Instability” [*North*, 1984]. Once the snow line drops to levels that can initiate ice caps in the Northern Hemisphere, small ice sheets grow quickly to substantial size and could survive subsequent warming perturbations. Whether this idealized

mechanism that is simply based on energy balance arguments and a temperature-dependent albedo parameterization is very efficient in stabilizing the glacial ice sheets in the Northern Hemisphere against strong changes of summer insolation is unclear at this stage. Another mechanism that may prevent an early meltdown of the MIS5 ice sheets is the long time lag of the ice sheet response to climate change, associated with the inertial mass of the ice sheet and the delayed bedrock response. Moreover, it has been argued [*Marshall and Clark*, 2002] that during MIS5 a substantial fraction of the early Laurentide ice sheet was frozen to the bedrock, which may have further stabilized the ice sheet against orbitally induced climate changes.

[38] Coupled models of glacial-interglacial cycles forced by orbital variations demonstrate that ice sheets can survive large precessional cycles in summer insolation during MIS5 [e.g., *Oerlemans*, 1980; *Gallée et al.*, 1992; *Abe-Ouchi et al.*, 2007]. In fact, also the IcIES model that was used to force LOVECLIM in experiment TR exhibits a slow but almost steady increase of ice volume during MIS5a–d. Whereas these model results suggest that the negative AMOC feedback identified in our study may not be necessary to build up ice sheets, it should also be mentioned that these models use relatively crude temperature forcings based on energy balance arguments and are not coupled to fully dynamical atmosphere-ocean models. Two recent fully coupled atmosphere–ocean–ice sheet model simulations [*Ganopolski et al.*, 2009; *Bonelli et al.*, 2009] demonstrate that precessionally induced meltwater pulses during MIS5a–d that are quite similar to those obtained from our diagnosed mass balance (Figure 5) may have in fact triggered a rapid disintegration of the Eurasian ice sheet [see *Ganopolski et al.*, 2009, Figure 4; *Bonelli et al.*, 2009, Figure 7] at 100 kyr and 78 kyr B.P.

[39] Our paper presents a new hypothesis for the long buildup phase of glacial ice sheets in the presence of large precessional-scale summer forcing. We conclude that the time scale of glacial cycles is controlled by external orbital forcing, positive feedbacks, frequently discussed in the literature, and negative feedbacks, as the one discussed, which could help to promote the buildup of glacial ice sheets during MIS5. The mechanism proposed here was inspired by paleoclimate reconstructions from the North Atlantic and Arctic region (Figures 1 and 2) and was quantitatively supported by climate modeling evidence (Figures 4, 5, and 7). However, more detailed sensitivity experiments need to be conducted with coupled ice sheet–climate models to develop a better understanding of the response of the coupled system (including oceanic response) to summer insolation changes.

[40] **Acknowledgments.** This research was supported by NSF grant ATM-0712690 and the Research Council of Norway (Leiv Eiriksson Mobility Program). Additional support was provided by the Japan Agency for Marine-Earth Science and Technology (JAMSTEC) and by NASA and NOAA through their sponsorship of research activities at the International Pacific Research Center. We thank David Hodell and one anonymous reviewer for their helpful and constructive comments.

References

Abe-Ouchi, A., T. Segawa, and F. Saito (2007), Climatic conditions for modelling the Northern Hemisphere ice sheets throughout the Ice Age cycle, *Clim. Past*, *3*, 423–438.

Berger, A. L. (1978), Long-term variations of daily insolation and Quaternary climatic changes, *J. Atmos. Sci.*, *35*(12), 2362–2367.

Bonelli, S., S. Charbit, M. Kageyama, M.-N. Woillez, G. Ramstein, C. Dumas, and A. Quiquet (2009), Investigating the evolution of major Northern Hemisphere ice sheets during the last glacial-interglacial cycle, *Clim. Past*, *5*, 329–345.

Capron, E., et al. (2010), Synchronising EDML and NorthGRIP ice cores using $\delta^{18}O$ of atmospheric oxygen ($\delta^{18}O_{atm}$) and CH_4 measurements over MIS5 (80–123 kyr), *Quat. Sci. Rev.*, *29*, 222–234.

Chapman, M., and N. J. Shackleton (1999), Ice-volume fluctuations, North Atlantic ice-rafting events, and deep-ocean circulation changes between 130 and 70 ka, *Geology*, *27*, 795–798.

Curry, W., and D. Oppo (1997), Synchronous, high-frequency oscillations in tropical sea surface temperatures and North Atlantic Deep Water production during the last glacial cycle, *Paleoceanography*, *12*, 1–14.

Dorale, J. A., B. P. Onac, J. Fornos, J. Ginés, A. Gines, P. Tuccimei, and D. Peate (2008), Sea-level highstand 81,000 years ago in Mallorca, *Science*, *327*, 860–863.

Driesschaert, E., T. Fichefet, H. Goosse, P. Huybrechts, I. Janssens, A. Mouchet, G. Munhoven, V. Brovkin, and S. L. Weber (2007), Modeling the influence of Greenland ice sheet melting on the Atlantic meridional overturning circulation during the nextmillennia, *Geophys. Res. Lett.*, *34*, L10707, doi:10.1029/2007GL029516.

Dyke, A., J. Andrews, P. Clarke, J. England, G. Miller, J. Shaw, and J. Veillette (2002), The Laurentide and Innuitian Ice Sheets during the Last Glacial Maximum, *Quat. Sci. Rev.*, *21*, 9–31.

Gallée, H., J. van Ypersele, T. Fichfet, I. Marsiat, C. Tricot, and A. Berger (1992), Simulation of the Last Glacial Cycle by a coupled, sectorially averaged climate-ice sheet model: 2. Response to insolation and CO_2 variations, *J. Geophys. Res.*, *97*(D14), 15,713–15,740.

Ganopolski, A., R. Calov, and M. Claussen (2009), Simulation of the last glacial cycle with a coupled climate ice-sheet model of intermediate complexity, *Clim. Past Discuss.*, *5*, 2269–2309.

Goosse, H., and T. Fichefet (1999), Importance of ice-ocean interactions for the global ocean circulation: A model study, *J. Geophys. Res.*, *104*(C10), 23,337–23,355.

Goosse, H., E. Deleersnijder, T. Fichefet, and M. England (1999), Sensitivity of a global coupled ocean-sea ice model to the parameterization of vertical mixing, *J. Geophys. Res.*, *104*(C6), 13,681–13,695.

Hays, J., J. Imbrie, and N. Shackleton (1976), Variations in the Earth's orbit: Pacemaker of the ice ages, *Science*, *194*, 1121–1132.

Indermühle, A., et al. (1999), Holocene carbon-cycle dynamics based on CO_2 trapped in ice at Taylor Dome, Antarctica, *Nature*, *398*, 121–126.

Knies, J., and C. Vogt (2003), Freshwater pulses in the eastern Arctic Ocean during Saalian and Early Weichselian ice-sheet collapse, *Quat. Res.*, *60*, 243–251.

Knies, J., J. Matthiessen, C. Vogt, S.-I. Nam, T. Fredrichs, A. Mackensen, and R. Stein (2007), Effects of arctic freshwater forcing on thermohaline circulation during the Pleistocene, *Geology*, *35*, 1075–1078.

Krinner, G., J. Mangerud, M. Jakobsson, M. Crucifix, C. Ritz, and J. Svendsen (2004), Enhanced ice sheet growth in Eurasia owing to adjacent ice-dammed lakes, *Nature*, *427*, 429–432.

Larsen, E., K. Kjaer, I. Demidov, S. Funder, K. Grøsfjeld, M. Houmark-Nielsen, M. Jensen, H. Linge, and A. Lyså (2006), Late Pleistocene glacial and lake history of northwestern Russia, *Boreas*, *35*, 394–424.

Mangerud, M., et al. (2004), Ice-dammed lakes and rerouting of the drainage of northern Eurasia during the Last Glaciation, *Quat. Sci. Rev.*, *23*, 1331–1332.

Marshall, S., and P. Clark (2002), Basal temperature evolution of North American ice sheets and implications for the 100-kyr cycle, *Geophys. Res. Lett.*, *29*(24), 2214, doi:10.1029/2002GL015192.

North, G. (1984), The small ice cap instability in diffusive climate models, *J. Atmos. Sci.*, *41*, 3390–3395.

North Greenland Ice Core Project Members (2004), High-resolution record of Northern Hemisphere climate extending into the last interglacial period, *Nature*, *431*, 147–151.

Oerlemans, J. (1980), Model experiments on the 100,000-yr glacial cycle, *Nature*, *287*, 430–432.

Oppenheimer, M. (1998), Global warming and the stability of the West Antarctic Ice Sheet, *Nature*, *393*, 325–332.

Oppo, D., L. Keigwin, J. McManus, and J. Cullen (2001), Persistent suborbital climate variability in marine isotope stage 5 and Termination II, *Paleoceanography*, *16*(3), 280–292.

Oppo, D., J. McManus, and J. Cullen (2006), Evolution and demise of the Last Interglacial warmth in the subpolar North Atlantic, *Quat. Sci. Rev.*, *25*, 3268–3277.

Peyaud, V., C. Ritz, and G. Krinner (2007), Modelling the Early Weichselian Eurasian Ice Sheets: Role of ice shelves and influence of ice-dammed lakes, *Clim. Past Discuss.*, *3*, 221–247.

Reeh, N. (1991), Parameterization of melt rate and surface temperature on the greenland ice sheet, *Polarfoschung*, *59*, 113–128.

Renssen, H., H. Goosse, T. Fichefet, V. Brovkin, E. Drieschaert, and F. Wolk (2005), Simulating the Holocene climate evolution at northern high latitudes using a coupled atmosphere-sea ice-ocean-vegetation model, *Clim. Dyn.*, *24*, 23–43.

Risebrobakken, B., T. Dokken, O. Ottera, E. Jansen, Y. Gao, and H. Drange (2007), Inception of the northern European ice sheet due to contrasting ocean and insolation forcing, *Quat. Res.*, *67*(1), 128–135.

Schmidt, M., H. Spero, and D. Lea (2004), Links between salinity variation in the Caribbean and North Atlantic thermohaline circulation, *Nature*, *428*, 160–163.

Siddall, M., E. J. Rohling, A. Almogi-Labin, C. Hemleben, D. Meischner, I. Schmelzer, D. A. Smeed (2003), Sea-level fluctuations during the last glacial cycle, *Nature*, *423*, 853–858.

Siegert, M., J. Dowdeswell, M. Hald, and J.-I. Svendsen (2001), Modelling the Eurasian Ice Sheet through a full (Weichselian) glacial cycle, *Global Planet. Change*, *31*, 367–385.

Smith, H. J., H. Fischer, M. Wahlen, D. Mastroianni, and B. Deck (1999), Dual modes of the carbon cycle since the Last Glacial Maximum, *Nature*, *400*, 248–250.

Spielhagen, R., K. Baumann, H. Erlenkeuser, N. Nowaczyk, N. Norgaard-Pedersen, C. Vogt, and D. Weiel (2004), Arctic Ocean deep-sea record of northern Eurasian ice sheet history, *Quat. Sci. Rev.*, *23*, 1455–1483.

Stouffer, R. J., et al. (2006), Investigating the causes of the response of the thermohaline circulation to past and future climate changes, *J. Clim.*, *19*, 1365–1387.

Stuiver, M., and P. Grootes (2000), GISP2 oxygen isotope ratios, *Quat. Res.*, *53*, 277–284.

Svendsen, J., et al. (2004), Late Quaternary ice sheet history of northern Eurasia, *Quat. Sci. Rev.*, *23*, 1229–1271.

Thompson, W., and S. Goldstein (2005), Open-system coral ages reveal persistent suborbital sea-level cycles, *Science*, *308*, 401–404.

Timm, O., and A. Timmermann (2007), Simulation of the last 21,000 years using accelerated transient boundary conditions, *J. Clim.*, *20*, 4377–4401.

Timm, O., A. Timmermann, A. Abe-Ouchi, T. Sewaga, and F. Saito (2008), On the definition of seasons in paleosimulations, *Paleoceanography*, *23*, PA2221, doi:10.1029/2007PA001461.

A. Abe-Ouchi, Atmosphere and Ocean Research Institute, University of Tokyo, 5-1-5, Kashiwanoha, Kashiwa-shi, Chiba 277-8568, Japan.

T. Friedrich, O. E. Timm, and A. Timmermann, IPRC, SOEST, University of Hawaii, 2525 Correa Rd., Honolulu, HI 96822, USA. (axel@hawaii.edu)

J. Knies, Geological Survey of Norway, N-7491 Trondheim, Norway.